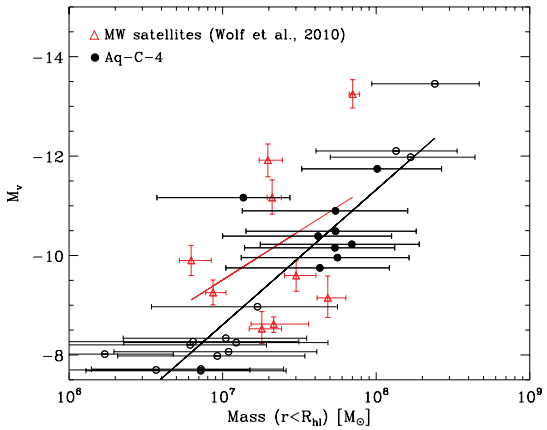

Figure 7. The total mass contained within the projected half-light radius ($R_{\rm hl}$) of simulated satellites, measured in the high-resolution, DMO, Aquarius-C-2 simulation (open and filled black circles). The radii are inferred from the observed luminosity–size relation (see text for details). The filled circles indicate those satellites that are used in the statistical comparison with the observed data, illustrated in Fig. 8. The error bars on the simulated data points show the masses obtained by assuming half-light radii 1σ above and below the mean fitted values, where σ is determined by the scatter about the fit to the observed data. Red crosses with error bars are estimates from Wolf et al. (2010) for a selection of MW satellites. Black and red lines show least-squares fits to the simulated and observed data points, respectively.

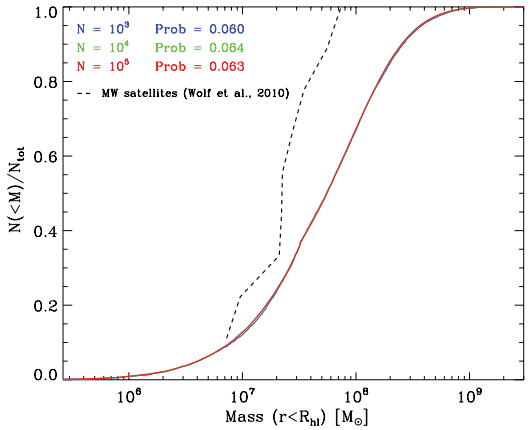

Figure 8. The cumulative fraction of the fourth to 12th brightest satellites as a function of the mass contained within the half-light radius in three model distributions (solid blue, green and red lines) and those derived for MW satellites by Wolf et al. (2010) (dashed line). Labels in the top left indicate the number of times we repeat the process of drawing masses for our sample of nine satellites in order to define the model distribution, along with the probability that each model is consistent with the observed masses.

to five times higher than the MW satellites of the same luminosity. While there is less of a discrepancy at fainter magnitudes, our model seems to show a more gradual increase in luminosity with mass than is suggested by the observational data. We note that, starting from identical initial conditions to our Aq-C-4 simulation, Wadepuhl & Springel (2011) found that the mass-to-light ratios of their satellites were typically higher than those quoted observationally by a very similar factor and were also more discrepant in the most massive satellites (see their fig. 15). In a hydrodynamic simulation of the Local Group, again with resolution similar to our Aq-C-4, Knebe et al. (2011a) found a similar result for satellites bound to their MW and M31 analogues, with mass-to-light ratios a factor $\sim$7 too high. We note, however, that they measured half-light radii for their satellites using the star particles forming in their simulation, which, as we have shown, can be too large when the scales associated with star formation are not resolved.

To quantify the discrepancy in Fig. 7 statistically, we construct multiple realizations of the half-light masses of the simulated satellites by drawing sizes from the distributions described above and computing the mass enclosed in the corresponding high-resolution Aquarius-C-2 satellites. We then combine the samples to define a model distribution for the cumulative fraction of satellites with mass larger than a given value and calculate the probability that the observed masses could have been drawn from it, using a one-tailed Kolmogorov–Smirnov (KS) test (Kolmogorov 1933; Smirnov 1939).

In order to make a like-for-like comparison with the results of Wolf et al. (2010), who did not measure masses for the Magellanic Clouds or Sagittarius, we exclude the three brightest simulated satellites from our analysis. At the faint end, our selection is dictated by resolution: we do not consider the faintest galaxies, i.e. those with fewer than 10 star particles. These choices restrict our sample to the fourth to 12th brightest satellites, which are indicated in Fig. 7 by filled circles. Note that the third brightest satellite in Aq-C-4 is in the midst of tidal disruption (see Section 6), a process that, as a result of small differences in the orbits of the subhaloes, is already complete in Aquarius-C-2, hence no counterpart is found. In Fig. 8, we plot cumulative model distributions, drawing masses for the sample of nine satellites multiple times to define each distribution, as indicated by the labels in the top left of the plot. The probability that the observationally derived masses are consistent with those distributions is found to be around 6 per cent. Note that this result is relatively insensitive to small changes in the luminosities of the satellites, such as those that may result from underestimating the effects of ram pressure stripping. Lower luminosities also decrease the half-light radius assigned to each satellite and hence the mass enclosed, moving the simulated points in Fig. 7 approximately parallel to the line of best fit.

As both Figs 7 and 8 demonstrate, the masses of the brightest simulated satellites are too high compared to those derived for the MW satellites. This is another manifestation of the problem recently highlighted by Boylan-Kolchin et al. (2011) who compared the measured masses within the half-light radii of the same satellites considered here with results from high-resolution simulations of CDM haloes, including the Aquarius suite. Assuming an NFW density profile (Navarro, Frenk & White 1996b, 1997), they showed that the most massive subhaloes in the simulations are too concentrated to be able to host the brightest observed satellites.

The mismatch seen in Fig. 7 and in the results of Boylan-Kolchin et al. (2011) could, in principle, be due to an underestimate of the central masses of the observed satellites. However, for the errors quoted by Wolf et al. (2010) to be substantially underestimated would require rather extreme variations in the anisotropy profile, which would be poorly fit by their fairly general parametrized form. This seems unlikely to be the sole source of the disagreement between model and data.

While the discrepancy could be simply due to statistics, it might also reflect a serious shortcoming either of the standard CDM cosmogony or of current models of galaxy formation, such as those assumed in our simulations. A possible explanation of the discrepancy between the mass-to-light ratios measured for the real and simulated satellites is that the central dark matter densities predicted in the CDM model are reduced by baryonic physics. One

mechanism for achieving this, proposed by Navarro et al. (1996a), is the condensation of a dense baryonic component followed by the rapid expulsion of gas by stellar feedback. The dark matter adjusts to this change in the potential by developing a central 'core', shifting the rotation curve maximum to a larger radius and reducing the mass-to-light ratio in the central parts. This process does indeed appear to play an important role in the evolution of one satellite in Aq-C-4 (see Section 6), which forms in the subhalo that has the largest mass prior to accretion. If this process is common, it is possible that it is not seen here in less massive subhaloes due to lack of resolution.

A more radical explanation of the discrepancy is that the dark matter consists of warm, rather than cold, particles. In this case, subhaloes of a given mass form later and have lower concentrations than in the CDM model (see Navarro et al. 1997; Hogan & Dalcanton 2000). Lovell et al. (2011) have recently shown explicitly that the masses and concentrations of subhaloes in a warm dark matter model agree well with the data.

6 A STAR-DOMINATED SATELLITE

The formation history of one of the satellite galaxies in our high-resolution hydrodynamical simulation is particularly interesting. By $z = 0$, we find that it has become dominated by its stellar component, with a mass-to-light ratio of $\sim$2.4 and its dark matter has become much less concentrated than otherwise similar subhaloes. It appears as an outlier in Fig. 6, as it has a very small half-light radius for its luminosity. In this section, we briefly describe its formation history and explain why it develops into such an unusual object.

At $z = 0$, the satellite is, in fact, in the process of being tidally disrupted and has a substantial stellar stream associated with it. Fig. 9 illustrates the structure of the stream in two orthogonal projections centred on the main galaxy. The dense stellar nucleus of the satellite that remains identifiable as a bound structure is also visible. We track all star particles associated with the satellite at the epoch when it is accreted and plot their projected mass density at $z = 0$. The stripped stars account for the majority of the stellar halo by mass.

The stream is a result of a fairly eccentric orbit with several close pericentres, illustrated in the bottom panel of Fig. 10, which shows the distance of the satellite from the centre of the main galaxy as a function of redshift. The dashed line indicates the virial radius of the main halo. The accretion time is the point where the two lines intersect. The top panel tracks the mass in gas, dark matter and stars bound to the satellite over the same redshift interval, as well as the total mass fraction in stars. At accretion, it is the brightest satellite of the central galaxy, but only the third brightest at $z = 0$, as a result of the reduction in stellar mass through tidal stripping. The stellar fraction at accretion ($\sim$0.02) is fairly typical of the surviving satellites. Note that it is very common for the stellar fraction of a satellite to increase with time after it is accreted, since the outer parts of the dark matter halo are less tightly bound than the stars and hence more susceptible to tidal stripping (e.g. Peñarrubia, Navarro & McConnachie 2008; Sawala et al. 2011). The middle panel of Fig. 10 shows the evolution of the central ($r < 1$ kpc) density of the subhalo in gas and dark matter, both of which drop sharply when the satellite is close to pericentre. A decline is also evident after $z \sim 3$, well before the satellite is accreted, the origin of which we discuss in more detail below.

During the first few orbits, the stellar component remains unaffected, while the dark matter lying beyond the radial extent of the stellar component is stripped. In fact, some of the dark matter particles with pericentres *within* the stellar component are also stripped, as a result of the dark matter having a higher radial velocity dispersion than the stars. The final masses of the stellar and dark matter components are factors of $\sim$50 and 2×10^4 lower than their peak values, respectively.

The extent to which the two components are stripped is strongly affected by their radial density profiles, which are shown in Fig. 11 at the time of accretion. The overplotted regions indicate the range of densities ($\pm 1\sigma$) in each bin for the nine most massive surviving satellites. Clearly, the stellar component of this galaxy is unusually concentrated relative to those other galaxies, whilst the dark matter

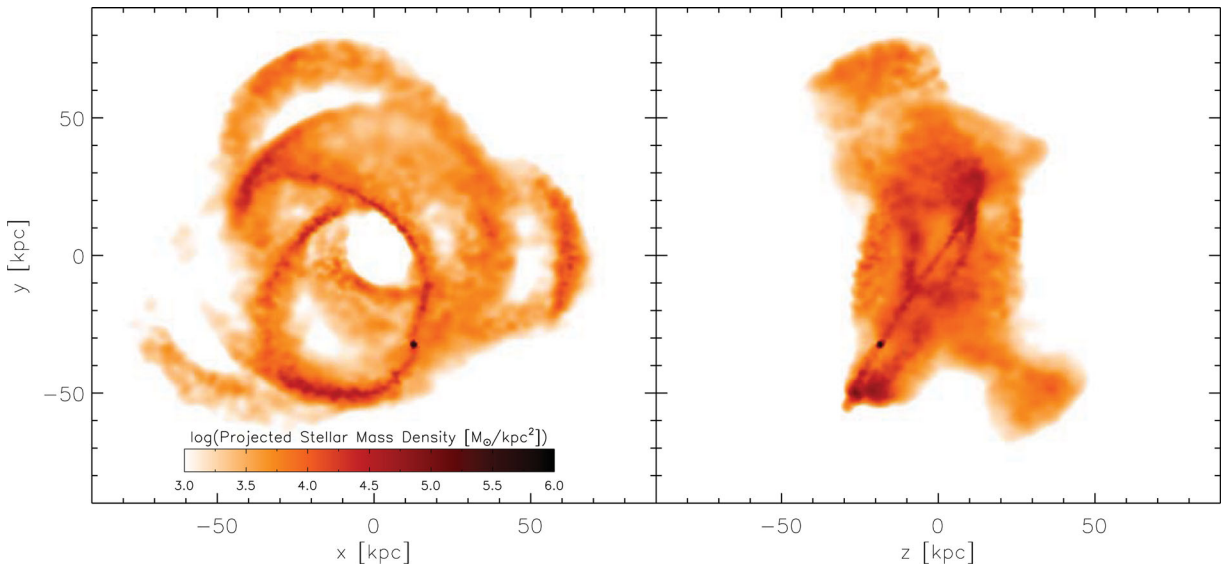

Figure 9. Two orthogonal projections through a cube of side 180 kpc, centred on the potential minimum of the main halo, showing the stellar stream associated with the satellite. Projected stellar mass density is plotted on a white–red–black scale as indicated by the colour bar. The stream is defined by selecting all stars associated with the satellite at the time of accretion and locating them at $z = 0$. The surviving satellite is clearly seen as the dark concentrated object lying along the stream.

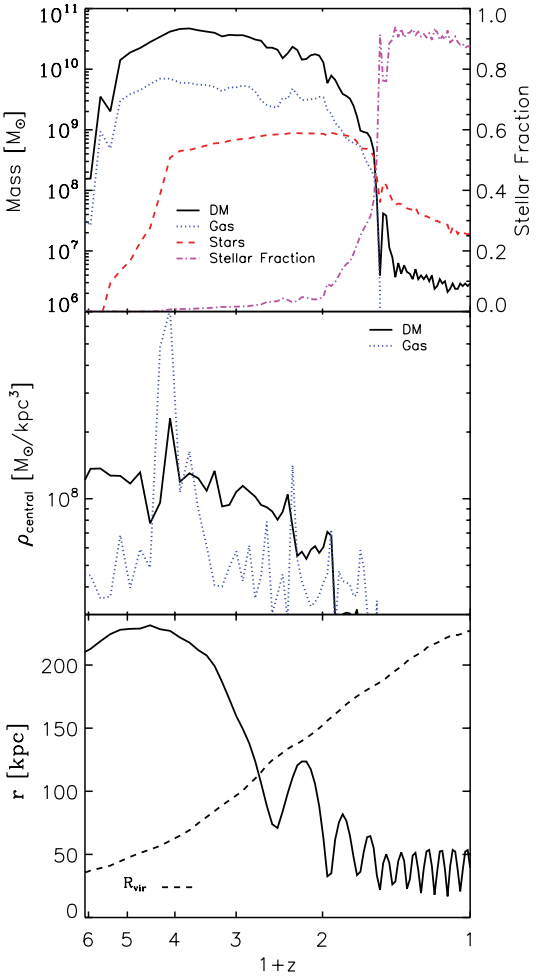

Figure 10. Top panel: the mass in dark matter (black, solid), gas (blue, dotted) and stars (red, dashed) gravitationally bound to the satellite's main progenitor, and the stellar fraction (magenta, dot–dashed, measured on the right vertical axis) as a function of redshift. Some of the small variations in the masses (and hence also the stellar fraction) at $z < 1$ are due to the difficulty in identifying the subhalo's particles against the high background density at the centre of the main halo. Centre panel: the density of dark matter (black, solid) and gas (blue, dotted) within the central 1 kpc. Bottom panel: the distance to the satellite from the centre of the main halo. The dashed line indicates the virial radius of the main halo.

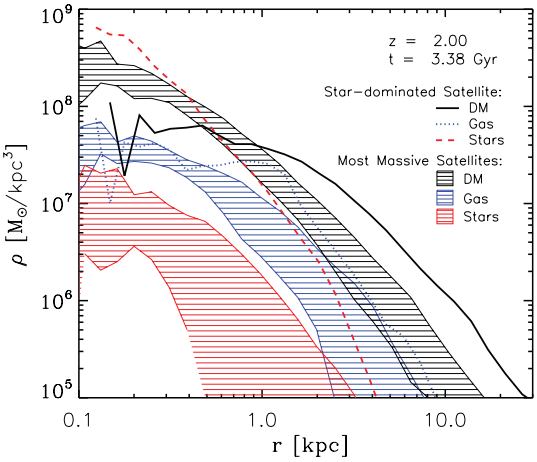

Figure 11. The dark matter (black, solid), gas (blue, dotted) and stellar (red, dashed) density profiles of the galaxy at $z \sim 2$, when it is first accreted as a satellite. Regions of the same colour indicate the spread of values ($\pm 1\sigma$) in each radial bin for the nine most massive surviving satellites at $z = 0$.

and gas have shallower than average central density profiles. It is unclear how much effect the gravitational softening has in this respect, since forces begin to become sub-Newtonian on scales less than $\lesssim$720 pc, but we note that the profiles also differ outside that radius. The highly 'cusped' stellar profile allows the central stellar nucleus to resist the strong tidal forces that unbind the majority of the dark matter. It also accounts for the unusually small half-light radius shown in Fig. 6.

The origin of these density profiles is related to the satellite's atypical formation history. In a series of major mergers at $z \sim 3$, gas is funnelled to the centre of the main progenitor, initiating an intense burst of star formation that gives rise to a highly concentrated stellar distribution. The subsequent burst of feedback energy rapidly removes a large fraction of the gas and leads to a fall in the mean binding energy of the central ($r < 1$ kpc) dark matter. This episode is clearly visible in the middle panel of Fig. 10, which shows the central gas density (blue curve) increases sharply and then drops back to the pre-merger value as gas is expelled by feedback and turned into stars, followed by a decline in the dark matter density (black curve) in response to the change in the potential. This sequence of events is effectively the process originally proposed by Navarro et al. (1996a). The reduced binding energy of its central dark matter, along with an extreme orbit, combine to produce the unusual properties of this satellite at $z = 0$.

7 CONCLUSIONS

We have investigated the formation and evolution of a MW-like satellite system in an SPH simulation over three levels of resolution, in which particle masses vary by a factor of 64. The properties of our simulated satellites show relatively good numerical convergence, with the final stellar masses typically agreeing to within a factor of 2, and always to within a factor of 6. We also compared to an independent estimate of the stellar mass expected to form in each subhalo, using the semi-analytical model of C10. The two theoretical techniques produce a similar ranking of the subhaloes by stellar mass, although our simulations typically form a higher mass of stars by a factor of between 2 and 6. This discrepancy may be partly explained by the assumption in the semi-analytical model that gas is stripped instantaneously when a galaxy becomes a satellite. The mass evolution in gas, stars and dark matter of each satellite agrees well between resolutions, except that gas is stripped more rapidly at lower resolution following accretion on to the main halo. Poorer force resolution causes gas particles to be more loosely bound to the subhalo and hence more susceptible to ram pressure stripping. This phenomenon may account for many of the differences in the final stellar masses between resolutions. Despite the inclusion of measures to improve SPH's modelling of contact instabilities, it is likely that our code still underestimates ram pressure stripping. Satellites will therefore retain more gas and form more stars after accretion than they should do.

By comparing the dark matter haloes of our satellite galaxies to those that form in a dissipationless version of the same simulation, we were able to quantify the expected impact of baryons on the phase-space structure of the dark matter. Due to small deviations in satellite orbits between different realizations of the same halo, it is necessary to make this comparison when the satellite first falls in rather than at $z = 0$. Although in some radial bins, in a few

subhaloes, the density and velocity dispersion profiles are found to change by ∼30 per cent, the differences were typically less than 10 per cent. With the caveat that the resolution of our simulation may limit the magnitude of such effects, we conclude that baryons have a relatively small impact on the structure of the dark matter haloes of satellite galaxies around MW-like hosts. We note that several previous studies have found that baryonic mechanisms can reduce the central dark matter densities of dwarf galaxies appreciably (e.g. Navarro et al. 1996a; El-Zant et al. 2001; Read & Gilmore 2005; Mashchenko et al. 2006; Goerdt et al. 2010; Governato et al. 2010); however, we find evidence for such effects only in one satellite. Our model provides a reasonable match to the faint end of the Local Group satellite luminosity function averaged between the MW and M31, although there is a slight deficit at the bright end, with no LMC analogue. However, SDSS data (Guo et al. 2011; Liu et al. 2011; Tollerud et al. 2011) suggest that it is quite common for galaxies with luminosities like the MW to have no satellites as bright as the LMC and SMC. The underestimation of ram pressure stripping and the corresponding overestimation of total stellar mass described above may increase the disagreement with the observations at the bright end. Effectively this means that less of the energy available from SNe would be required in order to match the observed satellite luminosity function.

Due to the limitations of the spatial resolution and the implementation of baryonic physics in our simulations, particularly the modelling of the multiphase ISM, stars do not form in sufficiently concentrated distributions to match the half-light radii of Local Group satellites. However, the reasonable agreement between the stellar masses in simulations with different resolution and different modelling techniques, combined with the match to the observed satellite luminosity function, suggests that the baryonic mass that is able to cool in each (sub)halo and form stars is realistic.

In order to test whether satellites of a given luminosity form in haloes with masses consistent with those observed, we compare their 'half-light masses' with values derived for a selection of the brightest MW satellites by Wolf et al. (2010). For this comparison, each satellite is assigned a distribution of half-light radii from the best fit to the observed luminosity–size relation and its variance. In the hydrodynamical simulation, the gravitational softening is comparable to these fitted half-light radii, so we instead measure the masses in a much higher resolution, DMO realization of the simulation. We hence explicitly ignore any effects baryons may have had on the central density profiles, which, in any case, the results in Section 3 suggest are small. The large scatter about the observed relation translates into a broad range of possible masses for each simulated satellite, but none the less, the mean masses for the brightest examples ($M_V < -11$) are about three to five times higher than their observed counterparts. The observed mass–luminosity relation seems to be somewhat steeper than that produced by our model, although due to the small sample sizes, the slope of the relation and the scatter about it are relatively poorly defined in both cases. A KS test, taking into account the uncertainties in the half-light radii assigned to the simulated satellites, returns a 6 per cent probability that the observed masses could have been drawn from the distribution defined by the simulation data. We note that this result is robust to small changes in the satellite luminosities due to the underestimation of ram pressure stripping; assigning a smaller half-light radius to a satellite also reduces the central mass measured, such that the discrepancy between the simulated and observed satellites remains.

Although the apparent disagreement between the simulations and the data could be simply due to statistics, there are also a number of plausible physical explanations. It could be that baryonic processes significantly reduce the central dark matter densities of satellite galaxies. Possible mechanisms to achieve this include, for instance, a sudden change in the local potential, induced by the rapid expulsion of baryonic mass through stellar feedback (e.g. Navarro et al. 1996a) or heating due to bulk motions of dense clumps of gas (e.g. Mashchenko et al. 2006). The results in Section 3 imply that, if such processes are important, they are either not resolved in the Aq-C-4 simulation or not properly captured by our feedback prescription, except in one case, which happens to be the most massive subhalo at accretion. Less concentrated dark matter profiles would also result if the dark matter consists of warm, rather than cold, particles (e.g. Lovell et al. 2011).

The broad range of possible explanations of the discrepancy highlighted by our results illustrates how uncertain our understanding of galaxy formation still is on the scale of dwarf galaxies. Determining which, if any, is correct will be of critical importance in assessing the viability of the CDM cosmology and the success of galaxy formation models.

ACKNOWLEDGMENTS

We thank Joop Schaye for helpful comments in the early stages of this work and Adrian Jenkins for creating the initial conditions for the simulations. We are also grateful to Andrew Cooper for giving us access to his semi-analytical satellite data and for helpful discussions. OHP acknowledges the receipt of an STFC studentship. TO acknowledges financial support by Grant-in-Aid for Scientific Research (S) by JSPS (20224002) and by Grant-in-Aid for Young Scientists (start-up: 21840015). Our thanks to the anonymous referee for several helpful suggestions that improved the manuscript. Simulations associated with this work were run on the IBM pSeries Power6 at the Rechenzentrum, Garching, the Cosmology Machine at the Institute for Computational Cosmology (ICC) in Durham, the Cray XT4 at the National Astronomical Observatory of Japan's Centre for Computational Astrophysics and at the Centre for Computational Sciences in the University of Tsukuba. CSF acknowledges a Royal Society Wolfson research merit award. We thank the DEISA Consortium (www.deisa.eu), co-funded through the EU FP6 project RI-031513 and the FP7 project RI-222919, for support within the DEISA Extreme Computing Initiative. This work was supported in part by an STFC rolling grant to the ICC and ERC Advanced Investigator grant 267291 COSMIWAY.

REFERENCES

Abel T., Haehnelt M. G., 1999, ApJ, 520, L13
Agertz O. et al., 2007, MNRAS, 380, 963
Bate M. R., Burkert A., 1997, MNRAS, 288, 1060
Belokurov V. et al., 2007, ApJ, 654, 897
Benson A. J., Frenk C. S., Lacey C. G., Baugh C. M., Cole S., 2002, MNRAS, 333, 177
Blumenthal G. R., Faber S. M., Flores R., Primack J. R., 1986, ApJ, 301, 27
Bothun G. D., Thompson I. B., 1988, AJ, 96, 877
Bower R. G., Benson A. J., Malbon R., Helly J. C., Frenk C. S., Baugh C. M., Cole S., Lacey C. G., 2006, MNRAS, 370, 645
Boylan-Kolchin M., Bullock J. S., Kaplinghat M., 2011, MNRAS, 415, L40
Ceverino D., Klypin A., 2009, ApJ, 695, 292
Ceverino D., Dekel A., Bournaud F., 2010, MNRAS, 404, 2151
Chabrier G., 2003, PASP, 115, 763
Cooper A. P. et al., 2010, MNRAS, 406, 744 (C10)
Dalla Vecchia C., Schaye J., 2008, MNRAS, 387, 1431
Davis M., Efstathiou G., Frenk C. S., White S. D. M., 1985, ApJ, 292, 371

Dehnen W., McLaughlin D. E., Sachania J., 2006, MNRAS, 369, 1688
Diemand J., Kuhlen M., Madau P., Zemp M., Moore B., Potter D., Stadel J., 2008, Nat, 454, 735
Dolag K., Borgani S., Murante G., Springel V., 2009, MNRAS, 399, 497
El-Zant A., Shlosman I., Hoffman Y., 2001, ApJ, 560, 636
El-Zant A. A., Hoffman Y., Primack J., Combes F., Shlosman I., 2004, ApJ, 607, L75
Elmegreen B. G., 1989, ApJ, 338, 178
Ferland G. J., Korista K. T., Verner D. A., Ferguson J. W., Kingdon J. B., Verner E. M., 1998, PASP, 110, 761
Fioc M., Rocca-Volmerange B., 1997, A&A, 326, 950
Font A. S. et al., 2011, MNRAS, 417, 1260
Frenk C. S., Evrard A. E., White S. D. M., Summers F. J., 1996, ApJ, 472, 460
Frenk C. S., White S. D. M., Bode P., Bond J. R., Bryan G. L., Cen R., Couchman H. M. P., Evrard A. E., 1999, ApJ, 525, 554
Fukui Y., Mizuno N., Yamaguchi R., Mizuno A., Onishi T., 2001, PASJ, 53, L41
Gelato S., Sommer-Larsen J., 1999, MNRAS, 303, 321
Gilmore G., Wilkinson M. I., Wyse R. F. G., Kleyna J. T., Koch A., Evans N. W., Grebel E. K., 2007, ApJ, 663, 948
Gnedin O. Y., Hernquist L., Ostriker J. P., 1999, ApJ, 514, 109
Gnedin O. Y., Kravtsov A. V., Klypin A. A., Nagai D., 2004, ApJ, 616, 16
Goerdt T., Moore B., Read J. I., Stadel J., Zemp M., 2006, MNRAS, 368, 1073
Goerdt T., Moore B., Read J. I., Stadel J., 2010, ApJ, 725, 1707
Governato F. et al., 2010, Nat, 463, 203
Guo Q., Cole S., Eke V., Frenk C., 2011, MNRAS, 417, 370
Haardt F., Madau P., 2001, in Neumann, D. M., Tran, J. T. V., eds, Clusters of Galaxies and the High Redshift Universe Observed in X-rays. Editions Frontières, Paris, p. 64
Heyer M. H., Carpenter J. M., Snell R. L., 2001, ApJ, 551, 852
Hilditch R. W., Howarth I. D., Harries T. J., 2005, MNRAS, 357, 304
Hoeft M., Yepes G., Gottlöber S., Springel V., 2006, MNRAS, 371, 401
Hogan C. J., Dalcanton J. J., 2000, Phys. Rev. D, 62, 063511
Katz N., Weinberg D. H., Hernquist L., 1996, ApJS, 105, 19
Kawata D., Okamoto T., Cen R., Gibson B. K., 2009, preprint (arXiv e-prints)
Kennicutt R. C., Jr, 1998, ApJ, 498, 541
Klypin A., Kravtsov A. V., Valenzuela O., Prada F., 1999, ApJ, 522, 82
Knebe A., Libeskind N. I., Knollmann S. R., Martinez-Vaquero L. A., Yepes G., Gottlöber S., Hoffman Y., 2011a, MNRAS, 412, 529
Knebe A. et al., 2011b, MNRAS, 415, 2293
Kolmogorov A., 1933, G. Istituto Ital. Attuari, 4, 83
Koposov S., Belokurov V., Evans N. W., Hewett P. C., Irwin M. J., 2008, ApJ, 686, 279
Li Y., White S. D. M., 2008, MNRAS, 384, 1459
Li Y., De Lucia G., Helmi A., 2010, MNRAS, 401, 2036
Liu L., Gerke B. F., Wechsler R. H., Behroozi P. S., Busha M. T., 2011, ApJ, 733, 62
Lovell M. et al., 2011, preprint (arXiv e-prints)
Macciò A. V., Kang X., Fontanot F., Somerville R. S., Koposov S., Monaco P., 2010, MNRAS, 402, 1995
McConnachie A. W. et al., 2008, ApJ, 688, 1009
Machacek M. E., Bryan G. L., Abel T., 2001, ApJ, 548, 509
Marigo P., 2001, A&A, 370, 194
Martin C. L., 2005, ApJ, 621, 227
Martin N. F., Ibata R. A., Irwin M. J., Chapman S., Lewis G. F., Ferguson A. M. N., Tanvir N., McConnachie A. W., 2006, MNRAS, 371, 1983
Mashchenko S., Couchman H. M. P., Wadsley J., 2006, Nat, 442, 539
Mashchenko S., Wadsley J., Couchman H. M. P., 2008, Sci, 319, 174
Mayer L., Governato F., Colpi M., Moore B., Quinn T., Wadsley J., Stadel J., Lake G., 2001, ApJ, 547, L123
Mihos J. C., Hernquist L., 1994, ApJ, 437, 611
Mo H. J., Mao S., 2004, MNRAS, 353, 829
Moore B., Ghigna S., Governato F., Lake G., Quinn T., Stadel J., Tozzi P., 1999, ApJ, 524, L19
Navarro J. F., White S. D. M., 1993, MNRAS, 265, 271
Navarro J. F., Eke V. R., Frenk C. S., 1996a, MNRAS, 283, L72
Navarro J. F., Frenk C. S., White S. D. M., 1996b, ApJ, 462, 563
Navarro J. F., Frenk C. S., White S. D. M., 1997, ApJ, 490, 493
Navarro J. F. et al., 2010, MNRAS, 402, 21
Okamoto T., Frenk C. S., 2009, MNRAS, 399, L174
Okamoto T., Jenkins A., Eke V. R., Quilis V., Frenk C. S., 2003, MNRAS, 345, 429
Okamoto T., Gao L., Theuns T., 2008, MNRAS, 390, 920
Okamoto T., Frenk C. S., Jenkins A., Theuns T., 2010, MNRAS, 406, 208
Peñarrubia J., Navarro J. F., McConnachie A. W., 2008, ApJ, 673, 226
Pietrzyński G. et al., 2009, ApJ, 697, 862
Pontzen A., Governato F., 2011, preprint (arXiv e-prints)
Portinari L., Chiosi C., Bressan A., 1998, A&A, 334, 505
Power C., Navarro J. F., Jenkins A., Frenk C. S., White S. D. M., Springel V., Stadel J., Quinn T., 2003, MNRAS, 338, 14
Price D. J., 2008, J. Comput. Phys., 2271, 10040
Read J. I., Gilmore G., 2005, MNRAS, 356, 107
Robertson B. E., Kravtsov A. V., 2008, ApJ, 680, 1083
Saitoh T. R., Makino J., 2009, ApJ, 697, L99
Samland M., Gerhard O. E., 2003, A&A, 399, 961
Sánchez-Salcedo F. J., Reyes Iturbide J., Hernandez X., 2006, MNRAS, 370, 1829
Sawala T., Scannapieco C., White S., 2011, preprint (arXiv e-prints)
Schaye J., Dalla Vecchia C., 2008, MNRAS, 383, 1210
Schaye J. et al., 2010, MNRAS, 402, 1536
Sijacki D., Vogelsberger M., Keres D., Springel V., Hernquist L., 2011, preprint (arXiv e-prints)
Smirnov N., 1939, Bul. Math. l'Universite Moscou, 2, 3
Solomon P. M., Rivolo A. R., 1989, ApJ, 339, 919
Somerville R. S., 2002, ApJ, 572, L23
Springel V., 2010, ARA&A, 48, 391
Springel V., Hernquist L., 2003, MNRAS, 339, 289
Springel V., White S. D. M., Tormen G., Kauffmann G., 2001, MNRAS, 328, 726
Springel V. et al., 2008, MNRAS, 391, 1685
Stadel J., Potter D., Moore B., Diemand J., Madau P., Zemp M., Kuhlen M., Quilis V., 2009, MNRAS, 398, L21
Stoehr F., White S. D. M., Tormen G., Springel V., 2002, MNRAS, 335, L84
Strigari L. E., Bullock J. S., Kaplinghat M., Kravtsov A. V., Gnedin O. Y., Abazajian K., Klypin A. A., 2006, ApJ, 652, 306
Strigari L. E., Frenk C. S., White S. D. M., 2010, MNRAS, 408, 2364
Tollerud E. J., Boylan-Kolchin M., Barton E. J., Bullock J. S., Trinh C. Q., 2011, ApJ, 738, 102
Truelove J. K., Klein R. I., McKee C. F., Holliman J. H., II, Howell L. H., Greenough J. A., 1997, ApJ, 489, L179
Wada K., Norman C. A., 2007, ApJ, 660, 276
Wadepuhl M., Springel V., 2011, MNRAS, 410, 1975
Walker M. G., Mateo M., Olszewski E. W., Gnedin O. Y., Wang X., Sen B., Woodroofe M., 2007, ApJ, 667, L53
Walker M. G., Mateo M., Olszewski E. W., Peñarrubia J., Wyn Evans N., Gilmore G., 2009, ApJ, 704, 1274
Watkins L. L., Evans N. W., An J. H., 2010, MNRAS, 406, 264
Wiersma R. P. C., Schaye J., Smith B. D., 2009a, MNRAS, 393, 99
Wiersma R. P. C., Schaye J., Theuns T., Dalla Vecchia C., Tornatore L., 2009b, MNRAS, 399, 574
Wolf J., Martinez G. D., Bullock J. S., Kaplinghat M., Geha M., Muñoz R. R., Simon J. D., Avedo F. F., 2010, MNRAS, 406, 1220
Xue X. X. et al., 2008, ApJ, 684, 1143
York D. G. et al., 2000, AJ, 120, 1579
Zucker D. B. et al., 2004, ApJ, 612, L121

This paper has been typeset from a TEX/LATEX file prepared by the author.